Chemistry
A European
Journal

Chemistry Europe
European Chemical Societies Publishing

Accepted Article

Title: Galactose Grafted Two-Dimensional Nanosheets as a Scaffold for the In-situ Synthesis of Silver Nanoparticles: A Potential Catalyst for the Reduction of Nitroaromatics

Authors: Kaloor S. Harikrishnan, Nithiyanandan Krishnan, Nilima Manoj Kumar, Anusree Krishna, Gowtham Raj, Devanathan Perumal, Jemshiya Kalathil, Jithu Krishna, and Reji Varghese

To be cited as: *Chem. Eur. J.* 10.1002/chem.202102421

Link to VoR: https://doi.org/10.1002/chem.202102421

WILEY-VCH

WILEY-VCH

FULL PAPER

Galactose Grafted Two-Dimensional Nanosheets as a Scaffold for the In-situ Synthesis of Silver Nanoparticles: A Potential Catalyst for the Reduction of Nitroaromatics

Kaloor S. Harikrishnan,† Nithiyanandan Krishnan,† Nilima Manoj Kumar, Anusree Krishna, Gowtham Raj, Devanathan Perumal, Jemshiya Kalathil, Jithu Krishna and Reji Varghese*

[a] Kaloor S. Harikrishnan,† Dr. Nithiyanandan Krishnan,† Nilima M. Kumar, Anusree Krishna, Gowtham Raj, Devanathan Perumal, Jemshiya Kalathil, Jithu Krishna and Dr. R. Varghese*
School of Chemistry
Indian Institute of Science Education and Research (IISER) Thiruvananthapuram
Thiruvananthapuram-695551, Kerala, India
E-mail: reji@iisertvm.ac.in
† These authors contributed equally

Supporting information for this article is given via a link at the end of the document.

Abstract: Two major hurdles in NP-based catalysis are the aggregation of the NPs and their recycling. Immobilization of NPs onto a 2D support is the most promising strategy to overcome these difficulties. Herein, amphiphilicity-driven self-assembly of galactose-hexaphenylbenzene based amphiphiles into galactose-decorated 2D nanosheet is reported. The extremely dense decoration of reducing sugar on the surface of the sheets is used for the in-situ synthesis and immobilization of ultrafine catalytically active AgNPs by using Tollens' reaction. The potential of the system as a catalyst for the reduction of various nitroaromatics is demonstrated. Enhanced catalytic activity is observed for the immobilized AgNPs when compared to the corresponding discrete AgNPs. Recovery of the catalytic system from the reaction mixture by ultrafiltration and its subsequent recycling for several cycles without dropping its activity is shown. This is the first report demonstrating the in-situ synthesis and immobilization of ultrafine AgNPs onto a 2D nanosheet that exhibits excellent catalytic performance for the reduction of nitroaromatics.

Introduction

High surface area to volume ratio provides remarkable chemical and physical properties to noble metal nanoparticles (NPs). By virtue of their unique properties they have found potential applications in various fields such as catalysis,[1] disease diagnosis,[2] therapy[3] and photonics.[4] Particularly, the area of heterogeneous catalysis has been greatly blessed by the advancements in the field of metal nanoparticle research.[5] Nevertheless, two major hurdles that are yet to be fully resolved in this field are the prevention of NPs aggregation during the reaction and their recyclability. Immobilization of NPs onto a 2D support is the most promising strategy for the prevention of NP aggregation and in many cases, this allows the recycling of the catalyst for several cycles without compromising the catalytic performance.[6] For example, graphene and graphene-based materials such as graphene oxide (GO) and reduced graphene oxide (rGO) have proven as excellent scaffolds for the immobilization of metal nanoparticles and remarkable catalytic performance have been achieved.[7] This is because they offer (i) extremely large surface area, (ii) strong interaction with the NPs (iii) possibility of modification of the electron density of the adsorbates and (iv) can favorably influence the kinetics of catalysis. In addition to graphene-based materials, metal-organic frameworks (MOFs), which can provide large surface area, tunable pore structures and tailorable functionalities, have also proven to be a promising scaffold for the organization of NPs for catalytic applications.[8] Other 2D supports including metal oxides,[9] hydrogels,[10] self-assembled nanostructures[11] etc. have also shown to be efficient as scaffolds for the immobilization catalytically active NPs. However, in all these cases immobilization of NPs onto the 2D support involves multiple steps and hence are highly laborious. Therefore, it is extremely desirable to have a simple design strategy that allows in-situ synthesis of NPs and their immobilization onto a 2D support in a single-step process.

Amphiphilicity-driven self-assembly is an efficient supramolecular approach for the crafting of self-assembled nanostructures of π-conjugated systems with well-defined morphology.[12] Sugar-based amphiphilic systems are particularly attractive as the nanostructures obtained from their self-assembly in aqueous medium offers a shell made of hydrophilic sugar moieties.[13] This subsequently permits sugar-directed chemistry on the surface of the nanostructures. Similarly, hexaphenylbenzene (HPB), a hydrophobe having large π-surface, have extensively explored for the design of amphiphiles owing to its high propensity to self-assemble via π-π stacking interaction.[14] Inspired from these examples, we envisaged that the incorporation of sugar as the hydrophilic unit to HPB could drive the self-assembly of the amphiphile in a lamellar fashion through the strong π-π stacking interaction of HPB to sugar-decorated 2D nanosheets. The protruding sugar moieties on the surface of the sheet then potentially permits sugar-guided chemistry on the sheet surface.

Herein, we report the self-assembly of a new class of amphiphiles having HPB as the hydrophobic segment and galactose as the hydrophilic units into galactose-decorated 2D nanosheet and demonstrates a single-step strategy for the in-situ synthesis and immobilization of catalytically active AgNPs as a catalyst for the reduction of nitroaromatics. Galactose is selected as the hydrophilic unit due to its ability to reduce Ag(I) ions to

10.1002/chem.202102421

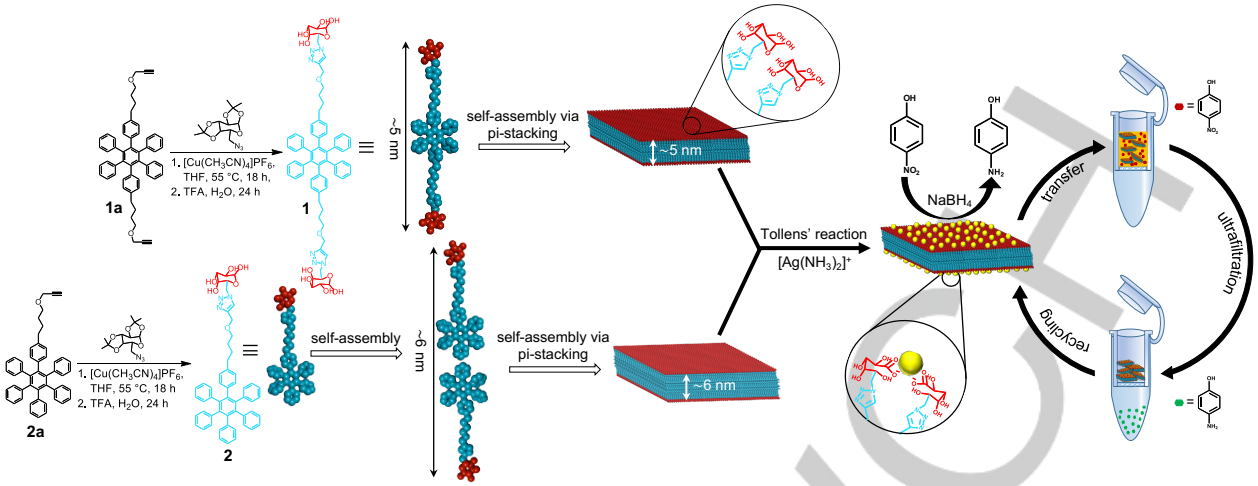

Scheme 1. Scheme for the syntheses of **1** and **2** and the schematic representation depicting the self-assembly of the amphiphiles into galactose-decorated 2D nanosheets. The in-situ synthesis of AgNPs using Tollens' reaction, their immobilization onto the sheet and the recycling of the catalytic system are also shown.

Ag(0), known as the Tollens' reaction. This reaction has been widely explored for the synthesis of AgNPs.[15] Accordingly, we designed two amphiphiles: (i) a bolaamphiphile having HPB as the hydrophobic segment and two galactose moieties symmetrically tethered as the hydrophilic units (**1**) and HPB as the hydrophobic segment and galactose as the hydrophilic segment (**2**). Both the amphiphiles undergo spontaneous self-assembly in aqueous medium via π–π stacking interaction of HPB into galactose-decorated 2D sheets. The protruding reducing sugar on the surface of the sheet is explored for the in-situ synthesis and immobilization of ultrafine catalytically active AgNPs by using Tollens' reaction. The potential of the system as a catalyst for the reduction of various nitroaromatics is demonstrated. Since the lateral dimension of the sheet is in the order of several micrometers, the catalytic system can easily be recovered from the reaction mixture by mere ultrafiltration, and the subsequent recycling of the catalyst for several cycles without dropping its activity is also demonstrated.

Results and Discussion

Syntheses of the amphiphiles

The amphiphiles **1** and **2** were synthesized using multistep organic reactions by a following reported procedure with appropriate modifications.[16] Initially, alcohol functionalized HPB derivatives (**1a** and **2a**) were synthesized through multistep organic reactions. The corresponding alcohol derivatives of HPB were then alkynylated (**1b** and **2b**) with propargyl bromide using NaH as base in DMF as the solvent. On the other hand, azide functionalized galactose (**3**) was synthesized by following a reported procedure. Subsequently, copper-catalyzed alkyne-azide cycloaddition (CuAAC) reaction between azide functionalized galactose and alkyne modified HPB derivative yielded the protected form of the amphiphiles. Deprotection using TFA:H_2O (1:1) furnished the corresponding amphiphiles **1** and **2** in reasonable yields (Scheme 1) . Experimental procedures and characterization details of **1**, **2** and all intermediates are provided in the Supporting Information.

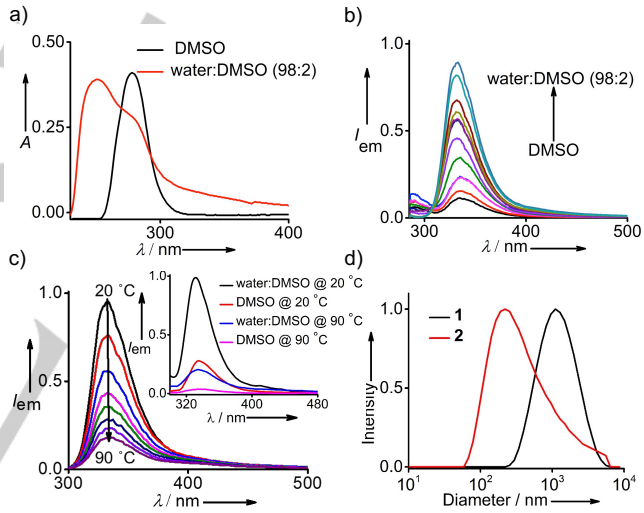

Figure 1. (a) UV-Vis absorption spectra of **1** in DMSO and water:DMSO (98:2). (b) Fluorescence spectral changes of **1** with the addition of water into its DMSO solution. (c) Temperature dependent fluorescence changes of **1** aggregate. Inset shows the comparison of spectral changes of the aggregates (water:DMSO) and monomeric species (DMSO) of **1** with respect to different temperatures. (d) DLS analysis of the aggregates of **1** and **2** in water:DMSO (98:2).

Self-assembly of the amphiphiles

Self-assembly of the amphiphiles (**1** and **2**) was achieved by adding water (980 μL) into a DMSO solution of **1** or **2** (100 μM, 20 μL), followed by annealing the solution at 90 °C for 10 minutes and subsequent slow cooling to room temperature. UV-visible absorption spectra of **1** (Figure 1a) and **2** (Figure S1) in DMSO showed the characteristic monomeric absorption of HPB with maximum centered at 270 nm, which corresponds to the π-π transition of HPB. Both the amphiphiles **1** and **2** exhibited very weak emission in DMSO λ_{ex} = 260 nm). Interestingly, an increase in emission intensity was observed with addition of water into their

DMSO solution with fluorescence quantum yields of 17 % and 18 % for **1** and **2**, respectively (Figure 1b and Figure S1). These results imply that **1** and **2** exist as monomeric species in DMSO and undergoes amphiphilicity-driven self-assembly with the addition of water into their DMSO solution mainly through π-π stacking of the HPB units. The nearly non-emissive nature of the monomeric species is due to the intramolecular $C(sp^2)$–$C(sp^2)$ bond rotational relaxation of the excited states of **1** and **2**. Whereas the intramolecular bond rotation is completely arrested in the aggregated state, which facilitate the radiative decay channel (fluorescence) of the excited states and thereby enhances the emission in the aggregated state. This phenomenon is known as aggregation induced enhanced emission (AIEE) and is very typical of HPB-based systems.[17] Temperature-dependent emission studies of the aggregates of **1** (Figure 1c) and **2** (Figure S2) in water:DMSO showed a decrease in emission intensity with the increase in temperature from 20 °C to 90 °C, and become almost non-emissive at high temperature. Moreover, emission intensity of **1** in water:DMSO (aggregated species) at 90 °C is nearly matching with the emission intensity of **1** in DMSO at 20 °C (monomeric species) (Figure 1c inset). These results confirm that the amphiphiles exist as aggregated species in water:DMSO at 20 °C and gradually breaks into the corresponding monomeric species upon rise in temperature. It is also to be noted a decrease in emission intensity of **1** in DMSO at 90 °C when compared to its emission intensity at 20 °C and this can be attributed to the mere effect of temperature on fluorescence (Figure 1c inset).[18] In support of this, dynamic light scattering (DLS) analyses of **1** and **2** solution in water:DMSO revealed the formation of aggregates with size distributions in the ranges of 250 nm–5 μm and 50 nm–6 μm for **1** and **2**, respectively (Figure 1d).

Detailed microscopic analyses were then carried out to understand the morphology of the aggregated species of **1** and **2**. Atomic force microscopic (AFM) analyses of the aggregates of **1** (Figure 2a) and **2** showed the formation of nanosheets with lateral dimensions in the range of several micrometers. Section analyses revealed that height of sheets of **1** is in the range of 20–100 nm (Figure 2a inset). Height of the sheet is significantly larger than the corresponding monolayer distance of **1** sheet (~5 nm), suggesting that the sheets are multilayered in nature. Scanning electron microscopic analyses of the aggregates of **1** (Figure 2b) and **2** (Figure S4) also showed the formation of multilayered sheets with lateral dimensions of several micrometers, which is in good agreement with the AFM analyses. Sheet morphology was further supported by transmission electron microscopic (TEM) analyses, which revealed the formation of highly transparent nanosheets for **1** (Figure 2c) and **2** (Figure S6). Furthermore, TEM analyses clearly disclosed the multilayered nature of the sheets (Figure 2d). All these results collectively conclude that both the amphiphiles undergo amphiphilicity-driven self-assembly mainly through π-π stacking interaction of HPB to micrometer-sized multilayered sheets. Accordingly, sheet of **1**, which is a bolaamphiphile, consists of monolayer assembly of **1** having π-stacked HPB as the hydrophobic core with hydrophilic galactose protruding on both the faces of the sheet as shown in Scheme 1. Similarly, sheet of **2**, which is an amphiphile, consist of bilayer assembly of HPB through π-π stacking as the hydrophobic core with hydrophilic galactose protruding on the faces of the sheet (Scheme 1).

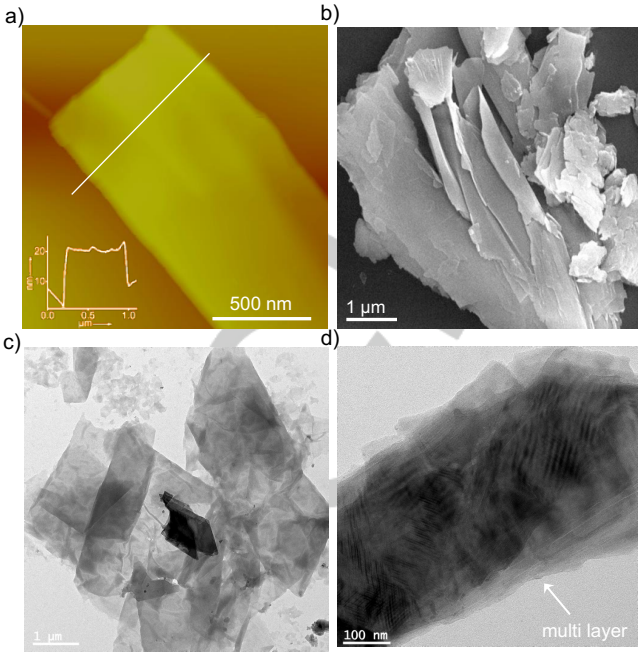

Figure 2. (a) AFM height, (b) SEM and (c) & (d) TEM images of **1** aggregates in water:DMSO (98:2). Inset of (a) shows the section analysis of the sheet along the line drawn on the image. [**1**] = 2 μM for all the experiments.

Synthesis of AgNPs and their immobilization onto the sheet

The most noteworthy structural feature of the sheets is the extremely dense display of reducing sugar on the surface of the sheets, which means that they offer a unique opportunity for the in-situ synthesis of AgNPs by using the well-known Tollens' reaction. Tollens' reaction involves the reduction of Ag(1) to Ag(0) by a reducing sugar such as galactose, which on the other hand undergoes oxidation of the aldehyde group to the corresponding carboxylic acid group. Subsequently, Ag(0) is acting as the seed for the growth of NPs of defined size and shape. For this purpose, Tollens' reagent ($[Ag(NH_3)_2]^+$) (20 mM) was added to the sheets of **1** or **2** (20 μM) in water:DMSO (98:2), vortexed for 2 h in dark. The in-situ formation of AgNPs was then followed by monitoring the emergence of surface plasmon absorption band of the NPs at 400 nm. Interestingly, UV-visible absorption spectrum of the solution of **1** sheet after 2h of reaction disclosed a strong absorption band with maximum centered at 400 nm, which clearly implies the in-situ formation of AgNPs (Figure 3a). In support of this, the colorless reaction mixture turned into pale yellow (Figure 3b). Furthermore, a significant quenching of fluorescence was observed for the sheets due to the electronic interaction between AgNPs formed on the sheet and HPB (Figure 3c), which is very much feasible as the distance separating them is only ~2.5 nm. Similar observations were seen for **2** sheets as well (Figure S7–S9).

To gain better insights into the structural characteristics of the NPs, detailed TEM analyses were carried out on the NPs obtained after the reactions of **1** and **2** sheets with Tollens' reagent. The TEM images of NPs in the case of **1** sheet revealed that the NPs are spherical in shape and nearly monodisperse (Figure 3d). The size of the NPs is in the range of 5–10 nm, which falls in the regime of ultrafine NPs (Figure 3d inset).[19] It is also obvious from the TEM images that the NPs are well-dispersed

10.1002/chem.202102421

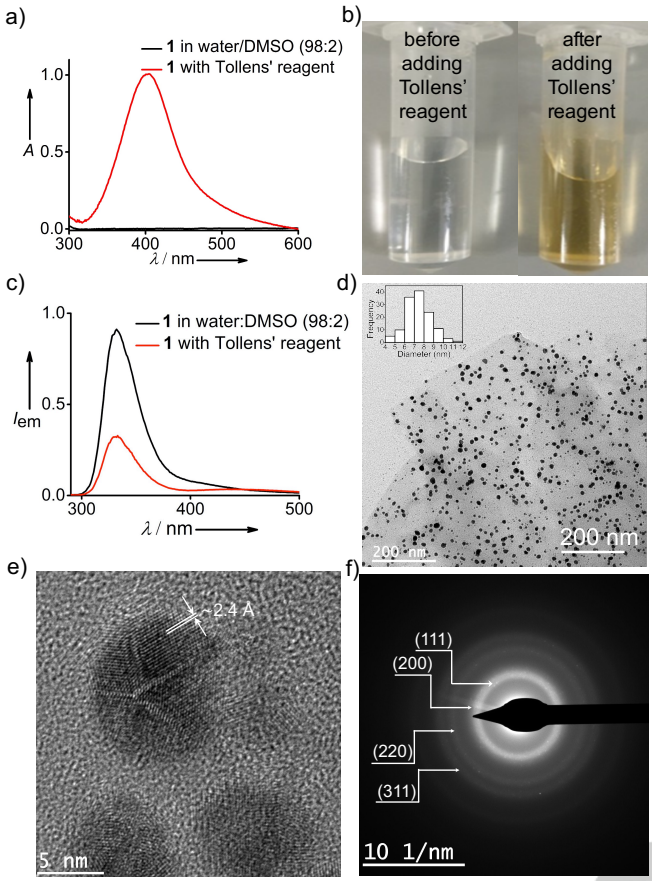

Figure 3. (a) UV-vis absorption spectra of **1** sheet before and after the addition of Tollens' reagent and (b) the corresponding colour changes of the solution. (c) Emission spectral changes before and after the addition of Tollens' reagent to the sheets of **1**. (d) TEM image of in-situ synthesized AgNPs on the surface of sheet of **1** and the inset shows the size distribution of the NPs constructed from the TEM data. (e) HR-TEM image of AgNPs and (f) the corresponding SAED pattern.

and supported on the sheet surfaces. Interestingly, the transparent sheet is also clearly visible in the TEM image, which unambiguously supports our hypothesis that galactose-decorated sheet is acting as the scaffold for the in-situ synthesis of AgNPs and their immobilization onto the sheet surface. The size of the AgNPs obtained was found to be independent of the concentration of the sheets. Furthermore, NPs immobilized on the sheet was found to be stable in the solution for several months without aggregation. Similar results were observed for the NPs obtained in the case **2** sheet as well. High resolution-TEM (HR-TEM) analysis clearly resolved the crystalline phase of the NPs with lattice fringe spacing of ~2.4 Å (Figure 3e). This corresponds to the (111) lattice plane of AgNPs. The corresponding selected area electron diffraction (SAED) studies further confirmed the crystalline nature of AgNPs with the characteristic Bragg peaks at (111), (200), (220) and (311) (Figure 3f). The electron energy loss spectroscopy (EELS) elemental mapping provided conclusive evidences for the hybrid nature of the nanostructure. As shown in Figure 4a, Ag and O elemental mapping mainly showed distribution on the NPs, which unequivocally confirm that the NPs are made of Ag and are stabilized by the COO^- ligands. As expected, C and N mapping revealed distribution along the

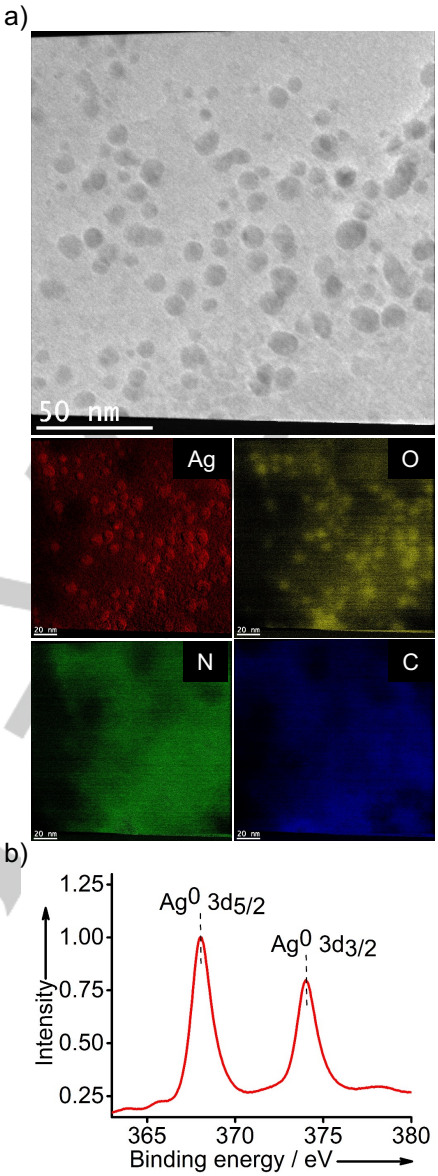

Figure 4. (a) EELS chemical composition maps and (b) XPS spectrum of **AgNP@1**.

underlying sheet. X-ray photoelectron spectroscopy (XPS) analyses confirmed the presence of Ag^0 NPs in NPs immobilized on **1** sheet (**AgNP@1**), where the characteristics binding energies of 368 eV ($3d_{5/2}$) and 374 eV ($3d_{3/2}$) of Ag^0 species were observed (Figure 4b).[13] These results confirm our hypothesis that galactose moieties grafted on the sheet surface is acting as a reducing agent for the reduction of Ag(1) to Ag(0) and the subsequent nucleation mediated growth of Ag(0) leading to the formation of AgNPs of defined size and shape. The in-situ formed NPs are stabilized on the sheet by the protruding carboxylic acid groups formed on the surface of the sheet after the Tollens' reaction.[20]

AgNP-decorated 2D nanosheet as a catalyst

10.1002/chem.202102421

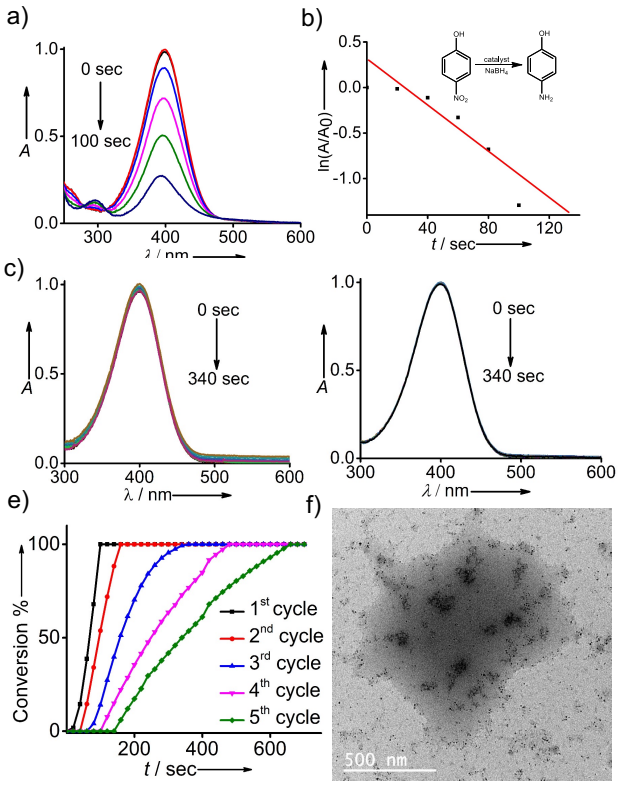

Figure 5. (a) Time dependent absorption spectral changes of reduction of 4-nitrophenol into 4-aminophenol using **AgNP@1** as the catalyst. (b) Reaction kinetics plot of 4-nitrophenol to 4-aminophenol using **AgNP@1** as the catalyst. Time dependent absorption spectral changes of reduction of 4-nitrophenol into 4-aminophenol using (c) discrete AgNPs and (d) **1** sheet as the catalysts. (e) Reaction kinetics using **AgNP@1** as the catalyst for different catalytic cycles. (f) TEM image of **AgNP@1** after the 5th cycle of the reaction.

The ultrafine size and hence the extremely high surface area to volume ratio of AgNPs motivated us to explore their potential as a catalyst for organic functional group transformation reactions. As a proof-of-concept, the catalytic performance of **AgNP@1** was studied for the reduction of nitroaromatics using $NaBH_4$ as the reducing agent. In order to compare the catalytic performance of the NPs immobilized on the sheet, similarly sized (~10 nm) AgNP was separately synthesized (citrate coated) and the reduction reactions were simultaneously carried out using this NPs as well. It must be noted that in all the reactions investigated, the concentrations of **AgNP@1** and $NaBH_4$ was adjusted in such a way that no reaction occurs when the reaction was carried out with discrete AgNP as the catalyst instead of **AgNP@1** while keeping all other experimental conditions same. Firstly, we investigated the reduction of 4-nitrophenol to 4-aminophenol. Typically, the reaction was performed by adding a freshly prepared cold aqueous solution of $NaBH_4$ (50 µL, 25 mM) to a solution of **AgNP@1** (20 µL, 20 µM) and 4-nitrophenol (250 µL, 150 µM) in 0.5 × TBE buffer. The reaction progress was then monitored by observing the intensity of the absorption peak of 4-nitrophenol at 400 nm. Interestingly, a gradual decrease in intensity of the peak with time and complete disappearance in 100 seconds was observed with the concomitant emergence of absorption peak corresponding to 4-aminophenol at 300 nm (Figure 5a). This clearly suggests the complete reduction of 4-nitrophenol to 4-aminophenol in 100 seconds. The residual absorption peak observed at 400 nm after completion of the reaction corresponds to the surface plasmon absorption of AgNPs, which is confirmed by comparing the absorption spectrum with a reaction mixture containing **AgNP@1** before adding 4-nitrophenol. On the contrary, no reduction in 100 seconds was observed when the reaction was carried out with discrete AgNPs as the catalyst instead of **AgNP@1** keeping all other experimental conditions same (Figure 5c). Furthermore, no catalytic activity was observed for **1** sheet (Figure 5d). This clearly shows the superior catalytic performance of **AgNP@1** when compared to their discrete counterparts. The reaction kinetics analysis showed that the reaction follows first order kinetics with a rate constant (k) of 12.0 × 10^{-3} s^{-1}. Similar enhanced catalytic activity was observed for **AgNP@1** for the reduction of other nitroaromatics too (Table 1).

Table 1. Reduction of nitroaromatics using **AgNP@1** as the catalyst

Entry	Substrate	T (ºC)	k (sec^{-1})
1	4-nitrophenol	RT	12.0 × 10^{-3}
2	2-nitrophenol	RT	3.29 × 10^{-3}
3	2-nitroaniline	RT	4.16 × 10^{-3}
4	4-amino-2-nitrophenol	RT	3.15 × 10^{-3}
5	4-amino-3-nitrophenol	RT	4.36 × 10^{-3}

Another remarkable characteristic of the **AgNP@1** is the ease of its recyclability. Because the lateral dimensions of the sheets are in the range of several micrometers, mere ultrafiltration (centrifugation at 12000 RPM) of the reaction mixture using a membrane filter (Amicon Ultra) permits the complete recovery of the catalyst. The catalyst was collected on the surface of the membrane whereas the product simply passed through the membrane. The recovered catalyst was reused for several cycles without comprising on the catalytic performance. It is to be noted that conversion rates above 99 % could be achieved for several cycles, however, longer reaction time was required with the increase in number of cycles. Reaction kinetics up to 5th cycles are provided in Figure 5e. The TEM image of the recycled **AgNP@1** catalyst was similar in nature to the TEM of the catalyst before the reaction, demonstrating the robustness of the catalyst. However, leaching of the NPs from the surface of the sheet and their aggregation were observed for the catalytic system after the 5th cycle as evident from the corresponding TEM image (Figure 5f). Leaching of the NPs after each cycle may be attributed to the mechanical force exerted during the centrifugation of the catalytic system for the recycling. This could be the reason for the drop in catalytic performance with the increase in the number of cycles.

Conclusions

In summary, we have reported the design and synthesis of two galactose-hexaphenylbenzene based amphiphiles that undergo self-assembly into high aspect ratio, galactose-decorated, 2D nanosheets. The most remarkable structural feature of the sheet is the extremely dense display of reducing sugar (galactose) on the surface of the sheet. We have demonstrated the potential of galactose-decorated nanosheets for the in-situ synthesis and immobilization of ultrafine AgNPs using Tollens' reaction. The in-situ formed NPs are stabilized by the protruding carboxylic acid

group formed on the surface of the sheet after Tollens' reaction. We have subsequently shown the potential of NP-decorated sheet as a catalyst for the reduction of a few nitroaromatics using $NaBH_4$ as the reducing agent. A significant enhancement in catalytic activity was observed for the immobilized catalysts when compared to their discrete counterparts. Since the lateral dimension of the sheet is in the micrometer regime, we were able to recover the catalyst by simple ultrafiltration using a membrane filter of appropriate pore size. The recovered catalyst was reused for several cycles without dropping the catalytic activity. However, longer reaction time was required with the increase in number of cycles due to the leaching of the NPs from the surface of the sheets. To the best of our knowledge, this is the first report demonstrating the in-situ synthesis and immobilization of catalytically active ultrafine AgNPs onto a 2D nanosheet that exhibits excellent catalytic performance for the reduction of nitroaromatics. Our results clearly demonstrate that amphiphilicity-driven self-assembly is a simple yet efficient strategy for the crafting of 2D nanostructures with tailorable functionalities and we hope this work will encourage the researchers to apply this strategy for the design of other catalytic systems.

Experimental Section

All chemicals used for the organic syntheses were purchased from Sigma Aldrich(http://www.sigmaaldrich.com/india.html). Solvents were dried using standard procedures. TLC analyses were done on aluminum plates coated with silica gel 60 F254, column chromatography was performed on 230-400 mesh silica gel. ^1H and ^{13}C NMR spectra were recorded on Bruker advanced 500 MHz DPX spectrometer using 1,1,1,1-tetramethylsilane (TMS) as the internal standard. Shimadzu IR prestige-21 FT-IR was used for recording IR spectra where solid samples were pelletized along with KBr. Water used for all studies was Milli-Q deionized water (18.2 MΩcm). AFM imaging was done on Multimode SPM (Veeco Nanoscope V). Samples were prepared by depositing 2 µL of aggregated samples on the freshly cleaved mica surface and were dried under air. Images were recorded under ambient conditions in tapping mode. The probe used for imaging was an antimony doped silicon cantilever with a resonance frequency of 300 kHz and a spring constant of 40 N m^{-1}. TEM analyses were carried out on an FEI Tecnai 30 G2 (300 kV) High Resolution-TEM with an embedded Quantum Gatan Image Filter (Quantum GIF) for EELS analyses. Sample preparation was done by drop-casting 2 µL of sample on a 400-mesh carbon-coated copper grid (Ted Pella, Inc.). The samples were allowed to adsorb on the grid for 2 min, and the excess sample was wicked with filter paper. XPS data were obtained using Omicron Nano tech. X-ray photoelectron spectrometer with Mg Kα x-ray (1253.6 eV). Absorption spectra were recorded on a Peltier attached Shimadzu UV-3600 Vis-NIR spectrophotometer in a quartz cuvette of 10 mm path length. Emission spectra were recorded on a Horiba Jobin Vyon Fluorimeter equipped with a Peltier cell holder. Temperature-dependent emission experiments were carried out by heating samples from 20 °C to 90 °C at an interval of 10 °C, equilibrating samples for 10 minutes at each temperature before recording the spectra and the solvents were given correction factors. DLS analyses were done on a Malvern Zetasizer Nano Zs equipped with a 655 nm laser. Experiments were performed at 25 °C at a backscattering angle of 173°. MALDI experiments were performed on Bruker UltrafleXtreme MALDI-TOF mass spectrometer.

Synthesis of 1: **Step1**: To a degassed suspension of **1a** (330 mg, 0.437 mmol) and isopropylidenegalactose azide (238.46 mg, 1.00 mmol) in anhydrous THF (20ml), $[Cu(CH_3CN)_4]PF_6$ (81.4 mg, 0.05 mol %) was added under N_2 atmosphere. The reaction was kept at 55 °C for 18 h. TLC has shown reaction completion and cooled down to room temperature and then the product was extracted with ethyl acetate. The organic layer separated was dried over anhydrous sodium sulphate and concentrated under reduced pressure to get the product protected product of **1**. The crude product thus obtained was purified by using Et_3N neutralized silica column chromatography using 50 % ethyl acetate. TLC (ethyl acetate:petroleum ether; 50:50) R_f = 0.48; Yield = 70%. ^1H NMR (500 MHz, $CDCl_3$): δ (ppm) = 7.607 (2H, s), 6.745–6.738 (20H, m), 6.617 (4H, d, J = 8 Hz), 6.554 (4H, d, J = 8 Hz), 5.427 (2H, d, J = 5 Hz), 4.570–4.508 (4H, m), 4.389–4.344 (2H, m), 4.260–4.245 (2H, m), 4.118 (4H, d, J = 8 Hz), 3.341 (4H, t, J = 6.5 Hz), 2.283 (4H, t, J = 7.5Hz), 1.419 (6H, s), 1.404–1.373 (4H, m), 1.326 (2H, s) 1.306 (8H, s), 1.284 (6H, s), 1.202 (6H, s); ^{13}C NMR (125 MHz, $CDCl_3$): δ(ppm) = 145.16, 140.79, 140.31, 140.23, 138.84, 138.01, 131.47, 131.28, 126.67, 126.50, 125.01, 123.71, 109.87, 109.05, 96.23, 71.15, 70.75, 70.356, 70.33, 67.24, 64.22, 50.47, 34.94, 28.66, 27.44, 25.98, 25.93, 24.90, 24.42. MALDI-TOF-m/z for $C_{80}H_{88}N_6O_{12}$: 1325.61 (calcd.); 1325.70 (expt.). **Step 2**: The protected derivative of **1** was then deprotected using 1:4 ratio of water:trifluoroacetic acid. This was achieved by keeping the reaction at 50 ºC for 24 h. Reaction completion was confirmed by TLC analysis and the reaction mixture was cooled down to room temperature. The crude product obtained was purified by column chromatography using 15 % methanol in chloroform to yield the product **1**. TLC (methanol:chloroform; 25:75); R_f = 0.48 Yield = 60 % .^1H NMR (500 MHz, DMSO-d_6): δ(ppm) = 7.939–7.910 (2H, m), 6.781–6.706 (20H, m), 6.6648 (4H, d, J = 7.9 Hz), 6.562 (4H, d, J = 8 Hz), 4.894 (1H, d, J=3.3 Hz), 4.825 (1H, d, J = 3.35 Hz), 4.399–4.337 (12H, m), 4.217–4.110 (7H, m), 3.810–3.785 (2H, m), 3.647–3.483 (2H, m), 3.531–3.483 (2H, m), 3.273–3.193 (6H, m), 2.223 (4H, t, J = 7.05 Hz), 1.299–1.269 (4H, m), 1.190-1.140 (4H, m). ^{13}C NMR (125 MHz, DMSO-d_6): δ (ppm) = 144.37, 140.51, 138.94, 138.03, 131.32, 126.97, 125.66, 124.89, 97.82, 93.15, 73.37, 72.07, 69.91, 69.37, 68.83, 63.76, 51.34, 34.56, 28.42, 27.53. MALDI-TOF-m/z for $C_{68}H_{72}N_6O_{12}$:1164.52 (calcd.); 1165.66 (expt.).

Synthesis of 2: **Step 1**: To a degassed suspension of **2a** (100 mg, 0.155 mmol) and isopropylidenegalactose azide (67 mg, 0.232 mmol) in anhydrous THF (10 ml), $[Cu(CH_3CN)_4]PF_6$ (4.3 mg, 0.05 mol%) was added under N_2 atmosphere. The reaction was kept at 55 °C for 18 h. TLC has shown reaction completion and cooled down to room temperature and then the product was extracted with ethyl acetate. The organic layer separated was dried over anhydrous sodium sulphate and concentrated under reduced pressure to get the protected derivative of **2**. The crude product thus obtained was purified by using Et_3N neutralized silica column chromatography using 50 % ethyl acetate in petroleum ether. TLC (ethyl acetate:petroleum ether; 50:50) R_f = 0.307, Yield = 70%. ^1H NMR (500 MHz, $CDCl_3$): δ (ppm) = 7.607 (1H, s), 6.775–6.746 (26H, m), 6.625 (2H, d , J = 8 Hz), 6.559 (2H, d, J = 8 Hz), 5.427 (1H, d, J = 4.5 Hz), 4.555 (2H, t, J = 8.5 Hz), 4.520 (2H, d, J = 10 Hz), 4.381 (1H, d, J = 8.5 Hz), 4.254 (1H, s), 4.117 (2H, d, J = 7.5 Hz), 3.342 (2H, t, J = 6.5 Hz), 2.285 (2H, t, J = 7.5 Hz), 1.419 (3H, s), 1.307 (4H, s), 1.284 (3H, s), 1.203 (4H, s); ^{13}C NMR (125 MHz, $CDCl_3$): δ(ppm) = 145.15, 140.72, 140.40, 140.23, 140.15,138.90, 137.96, 131.45, 131.27, 126.70, 126.55, 126.53, 125.14, 125.07, 123.73, 109.88, 109.06, 96.23, 71.16, 70.76, 70.36,70.34,67.25, 64.22, 50.49, 34.95, 29.72, 28.66, 27.44, 25.99, 25.94, 24.91, 24.42. MALDI-TOF-m/z for $C_{61}H_{59}N_3O_6$: 929.44 (calcd.); 929.93 (expt.). **Step 2**: The deprotected product of **2** was then deprotected using 1:4 ratio of water:trifluoroacetic acid. The reaction was kept at 50 °C for 24 h. TLC shown reaction completion and cooled down to room temperature to yield **2**. The crude product obtained was purified by column chromatography using 15 % methanol in chloroform. TLC (methanol:chloroform; 25:75), R_f = 0.32, Yield = 50%. ^1H NMR (500 MHz, DMSO-d_6): δ(ppm) = 7.927 (1H, t, J=7.5), 7.753 (25H, m), 6.674 (2H, d, J = 7.5 Hz), 6.568 (2H, d, J = 7.5

Hz), 4.383 (4H, m), 4.185 (1H, m), 3.801 (1H, t, J = 6 Hz), 3.637 (2H, d, J = 5 Hz), 2.226 (2H, s), 1.218 (5H, m). ^{13}C NMR (125 MHz, DMSO-d_6): δ(ppm) = 140.63, 140.50, 140.34, 138.97, 131.37, 131.22, 127.02, 126.96, 125.75,125.68, 69.36, 63.75, 34.55, 28.40, 27.51. MALDI-TOF-m/z for $C_{55}H_{51}N_3O_6$: 849.37 (calcd.); 849.93 (expt.).

Acknowledgements

The authors thank the DBT (BT/PR30172/NNT/28/1593/- 2018) for financial support. The authors are grateful to CSIR (K. S. H., D. P., and J. K.) and UGC (N. K.) for research fellowships.

Keywords: amphiphiles • supramolecular chemistry • 2D nanosheet • Tollens' reaction • catalysis

[1] D. Astruc, F. Lu, J. R. Aranzaes, *Angew. Chem. Int. Ed*. **2005**, *44*, 7852.

[2] A. B. Chinen, C. M. Guan, J. R. Ferrer, S. N. Barnaby, T. J. Merkel, C. A. Mirkin, *Chem. Rev*. **2015**, *115*, 10530.

[3] E. C. Dreaden, A. M. Alkilany, X. Huang, C. J. Murphy, M. A. El-Sayed, *Chem. Soc. Rev*. **2012**, *41*, 2740.

[4] N. Li, Y. Shang, Z. Han, T. Wang, Z.-G. Wang, B. Ding, *ACS Appl. Mater. Interfaces* **2019**, *11*, 13835.

[5] a) S. M. Ansar, C. L. Kitchens, *ACS Catal*. **2016**, *6*, 5553; b) J. Schçbel, M. Burgard, C. Hils, R. Dersch, M. Dulle, K. Volk, M. Karg, A. Greiner, H. Schmalz, *Angew. Chem. Int. Ed.* **2016**, *56*, 405; c) L. Liu, A. Corma, *Chem. Rev*. **2018**, *118*, 4981.

[6] a) K. Jasuja, J. Linn, S. Melton, V. Berry, *J. Phys. Chem. Lett*. **2010**, *1*, 1853; b) X. Wang, S. M. Tabakman, H. Dai, *J. Am. Chem. Soc*. **2008**, *130*, 8152; c) Q.-L. Zhu, Q. Xu, *Chem* **2016**, *1*, 220; d) L. Shao, X. Huang, D. Teschner, W. Zhang, *ACS Catal*. **2014**, *4*, 2369.

[7] a) S. Navalon, A. Dhakshinamoorthy, M. Alvaro, H. Garcia, *Coord. Chem. Rev*. **2016**, *312*, 99; b) S. Navalon, A. Dhakshinamoorthy, M. Alvaro, H. Garcia, *Chem. Rev*. **2014**, *114*, 6179.

[8] a) R. Yan, Y. Zhao, H. Yang, X.-J. Kang, C. Wang, L.-L. Wen, Z.-D. Lu, *Adv. Funct. Mater*. **2018**, *28*, 1802021; b) J. Nicks, K. Sasitharan, R. R. R. Prasad, D. J. Ashworth, J. A. Foster, *Adv. Funct. Mater*. **2021**, 2103723

[9] J. Azadmanjiri, V. K. Srivastava, P. Kumar, J. Wang, A. Yu, *J. Mater. Chem. A* **2018**, *6*, 13509.

[10] A. Zinchenko, Y. Miwa, L. I. Lopatina, V. G. Sergeyev, S. Murata, *ACS Appl. Mater. Interfaces* **2014**, *6*, 3226.

[11] N. Krishnan, M. Golla, H. V. P. Thelu, S. K. Albert, S. Atchimnaidu, D. Perumal, R. Varghese, *Nanoscale* **2018**, *10*, 17174.

[12] a) F. J. M. Hoeben, I. O. Shklyarevskiy, M. J. Pouderoijen, H. Engelkamp, A. P. H. J. Schenning, P. C. M. Christianen, J. C. Maan, E. W. Meijer, *Angew. Chem. Int. Ed*. **2006**, *45*, 1232; b) J. P. Hill, W. Jin, A. Kosaka, T. Fukushima, H. Ichihara, T. Shimomura, K. Ito, T. Hashizume, N. Ishii, T. Aida, *Science* **2004**, *304*, 1481; c) J. F. Hulvat, M. Sofos, K. Tajima, S. I. Stupp, *J. Am. Chem. Soc*. **2005**, *127*, 366; d) D.-W. Lee, T. Kim, M. Lee, *Chem. Commun*. **2011**, *47*, 8259; e) M. A. Azagarsamy, P. Sokkalingam, S. rmanavan, *J. Am. Chem. Soc*. **2009**, *131*, 14184; f) B. Narayan, S. P. Senanayak, A. Jain, K. S. Narayan, S. J. George, *Adv. Funct. Mater*. **2013**, *23*, 3053; g) C. Rest, M. J. Mayoral, K. Fucke, J. Schellheimer, V. Stepanenko, G. Fernández, *Angew. Chem. Int. Ed*. **2014**, *53*, 700; h) X. Zhang, D. Görl, V. Stepanenko, F. Würthner, *Angew. Chem. Int. Ed*. **2014**, *53*, 1270; i) S. Yagai, S. Okamura, Y. Nakano, M. Yamauchi, K. Kishikawa, T. Karatsu, A. Kitamura, A. Ueno, D. Kuzuhara, H. Yamada, T. Seki, H. Ito, *Nat. Commun.* **2014**, *5*, 4013; j) S. Ghosh, D. S. Philips, A. Saeki, A. Ajayaghosh, *Adv. Mater.* **2017**, *29*, 1605408; k) G. Das, S. Cherumukkil, A. Padmakumar, V. B. Banakar, V. K. Praveen, A. Ajayaghosh, *Angew. Chem. Int. Ed*. **2021**, *60*, 7851; l) S. Bej, A. Dhayani, P. Vemula, S. Ramakrishnan, *Langmuir* **2021**, *37*, 1788; m) A. Mukherjee, T. Sakurai, S. Seki, S. Ghosh, *Langmuir* **2020**, *36*, 13096; n) A. Mal, S. Vijayakumar, R. K. Mishra, J. Jacob, R. S. Pillai, D. Kumar B. S., A. Ajayaghosh, *Angew. Chem. Int. Ed*. **2020**, *59*, 8713; o) S. S. Babu, V. K. Praveen, A. Ajayaghosh, *Chem. Rev*. **2014**, *114*, 1973; p) F. García, G. Fernández, L. Sánchez, *Chem. Eur. J.* **2009**, *15*, 6740; q) F. García, L. Sánchez, *Chem. Eur. J.* **2010**, *16*, 3138; r) V. S. Talens, P. Englebienne, T. T. Trinh, W. E. M. Noteborn, I. K. Voets, R. E. Kieltyka, *Angew. Chem. Int. Ed.* **2015**, *54*, 10502.

[13] a) J.-H. Ryu, E. Lee, Y.-b. Lim, M. Lee, *J. Am. Chem. Soc*. **2007**, *129*, 4808; b) S. R. Jadhav, P. K. Vemula, R. Kumar, S. R. Raghavan, G. John, *Angew. Chem. Int. Ed.* **2010**, *49*, 7695; c) J. H. Jung, Y. Do, Y.-A. Lee, T. Shimizu, *Chem. Eur. J.* **2005**, *11*, 5538; d) K.-R. Wang, H.-W. An, L. Wu, J.-C. Zhang, X.-L. Li, *Chem. Commun*. **2012**, *48*, 5644; e) G. Yu, Y. Ma, C. Han, Y. Yao, G. Tang, Z. Mao, C. Gao, F. Huang, *J. Am. Chem. Soc*. **2013**, *135*, 10310.

[14] a) V. Vij, V. Bhalla, M. Kumar, *Chem. Rev*. **2016**, *116*, 9565; b) M. Golla, S. K. Albert, S. Atchimnaidu, D. Perumal, N. Krishnan, R. Varghese, *Angew. Chem. Int. Ed*. **2019**, *58*, 3865;

[15] a) G. A. Burley, J. Gierlich, M. R. Mofid, H. Nir, S. Tal, Y. Eichen, T. Carell, *J. Am. Chem. Soc*. **2006**, *128*, 1398; b) S. Pal, R. Varghese, Z. Deng, Z. Zhao, A. Kumar, H. Yan, Y. Liu, *Angew. Chem. Int. Ed*. **2011**, *50*, 4176; c) R. Dondi, W. Su, G. A. Griffith, G. Clark, G. A. Burley, *Small* **2012**, *8*, 770.

[16] D. Marinelli, F. Fasano, B. Najjari, N. Demitri, D. Bonifazi, *J. Am. Chem. Soc*. **2017**, *139*, 5503.

[17] S. Pramanik, V. Bhalla, H. M. Kim, H. Singh, H.W. Lee, M. A. Kumar, *Chem. Commun*. **2015**, *51*, 15570.

[18] S. K. Albert, M. Golla, H. V. P. Thelu, N. Krishnan, P. Deepak, R. Varghese, *Org. Biomol. Chem*. **2016**, *14*, 6960.

[19] H.-Lei Cao, H.-B. Huang, Z. Chen, B. Karadeniz, J. Lü, R. Cao, *ACS Appl. Mater. Interfaces* **2017**, *9*, 5231.

[20] O. Sambalova, K. Thorwarth, N. V. Heeb, D. Bleiner, Y. Zhang, A. Borgschulte, A. Kroll, *ACS Omega* **2018**, *3*, 724.

10.1002/chem.202102421

Entry for the Table of Contents

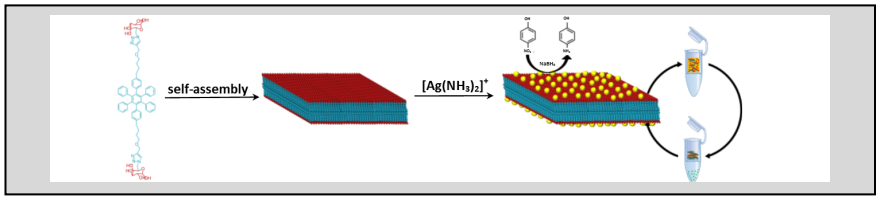

Amphiphilicity-driven self-assembly of galactose-hexaphenylbenzene based amphiphiles into galactose-decorated 2D nanosheet is reported. The extremely dense decoration of reducing sugar on the surface of the sheets is used for the in-situ synthesis and immobilization of ultrafine catalytically active AgNPs by using Tollens' reaction. The potential of the system as a recyclable catalyst for the reduction of various nitroaromatics is demonstrated. Enhanced catalytic activity is observed for the immobilized AgNPs when compared to the corresponding discrete AgNPs.